



# Constraining the Solar System’s Debris Disk with In Situ *New Horizons* Measurements from the Edgeworth–Kuiper Belt

A. R. Poppe<sup>1,8</sup> , C. M. Lisse<sup>2</sup> , M. Piquette<sup>3,8</sup>, M. Zemcov<sup>4</sup> , M. Horányi<sup>5,8</sup>, D. James<sup>5,8</sup>, J. R. Szalay<sup>6,8</sup>, E. Bernardoni<sup>5,8</sup>, and S. A. Stern<sup>7,8</sup>

<sup>1</sup> Space Sciences Laboratory, University of California at Berkeley, 7 Gauss Way, Berkeley, CA 94720, USA; [poppe@ssl.berkeley.edu](mailto:poppe@ssl.berkeley.edu)

<sup>2</sup> Johns Hopkins University Applied Physics Laboratory, Laurel, MD, USA

<sup>3</sup> Laboratory for Atmospheric and Space Physics, University of Colorado at Boulder, Boulder, CO 80309, USA

<sup>4</sup> Center for Detectors, School of Physics and Astronomy, Rochester Institute of Technology, 1 Lomb Memorial Drive, Rochester, NY 14623, USA

<sup>5</sup> Department of Physics and Laboratory for Atmospheric and Space Physics, University of Colorado at Boulder, Boulder, CO 80309, USA

<sup>6</sup> Department of Astrophysical Sciences, Princeton University, Princeton, NJ, USA

<sup>7</sup> Southwest Research Institute, Boulder, CO, USA

Received 2019 June 26; revised 2019 July 12; accepted 2019 July 15; published 2019 August 7

## Abstract

The solar system currently possesses two remnant debris disks leftover from the planetary formation era in the form of the asteroid belt and the Edgeworth–Kuiper Belt (EKB). Similar to other stellar systems, these debris disks continually generate submillimeter-sized dust grains through processes such as mutual collisions, interstellar dust grain bombardment, and sublimation/sputtering of larger grains. Here, we use recent in situ measurements by the *New Horizons* Student Dust Counter and an interplanetary dust dynamics model to constrain the overall structure and magnitude of the solar system’s debris disk, including the disk mass, optical depth, and surface brightness in both scattered light and thermal emission. We find that  $\sim 99\%$  of the solar system’s dust disk mass (grains with diameter  $< 1$  mm) is contained within EKB and Oort Cloud cometary grains outside of 30 au, with the remaining  $\sim 1\%$  mass in the form of Jupiter-family cometary dust within 5 au. The total disk mass is estimated to be  $\sim 8 \times 10^{-7} M_{\oplus}$  with a total fractional luminosity of  $\sim 5 \times 10^{-7}$ , confirming our solar system as a relatively dust-poor system compared to debris disks around similar-aged FGK stars. Finally, we estimate that Kuiper Belt Object collisional events such as that which created the Haumea family could transiently increase the current surface brightness of our debris disk by a factor of only  $\sim 6$ , far less than median brightnesses seen in other nearby disks. This further supports the idea that the EKB has been largely depleted of its primordial mass relative to other stellar systems by instabilities triggered by planetary migration.

*Unified Astronomy Thesaurus concepts:* [Kuiper Belt \(893\)](#); [Debris disks \(363\)](#); [Interplanetary dust \(821\)](#)

## 1. Introduction

Debris disks are collections of nanometer- to millimeter-sized dust grains sourced from planetesimals leftover from planetary formation epochs in stellar systems (e.g., Kral et al. 2017; Hughes et al. 2018). Debris disks are believed to be actively sourced from a combination of collisional grinding of remanent planetesimals, outgassing of material from cometary bodies, and sublimation/sputtering of larger-sized grains, with relatively rapid loss of material due to Poynting–Robertson and stellar wind drag, gravitational perturbations with planetary objects, and grain–grain mutual collisions (e.g., Burns et al. 1979; Gustafson 1994; Borkowski & Dwek 1995). The first observations of exozodiacal debris disks appeared as thermal excesses in *IRAS* measurements of nearby stars (Aumann et al. 1984; Aumann 1985) and since then have been detected from optical to millimeter wavelengths around hundreds of stars. Studies of debris disks inform us about processes that lead to protoplanetary and planetary formation as well as processes that continue to erode planetary systems away. Understanding debris disk structure can also reveal, albeit indirectly, the presence and dynamics of planetary objects in stellar systems via the introduction of structures such as narrow and/or confined rings, asymmetric clumps, and out-of-plane warping in debris disks (e.g., Greaves et al. 1998, 2005; Wyatt et al. 1999; Wyatt 2003; Stark & Kuchner 2008; Chiang et al. 2009).

Knowledge of our own solar system’s debris disk (or interplanetary dust distribution) has been informed by both remote-sensing and in situ measurements. Scattered light and thermal emission observations of “zodiacal light” have constrained the overall brightness and structure near 1 au (e.g., Hauser et al. 1984; Reach et al. 1996, 2003; Kelsall et al. 1998; Fixsen & Dwek 2002; Hahn et al. 2002; Maris et al. 2006; Planck Collaboration et al. 2014; Dikarev & Schwarz 2015; Kondo et al. 2016) and through the asteroid belt (Hanner et al. 1974). Comparison of dynamical interplanetary dust models to these observations suggest that much of the interplanetary dust distribution at 1 au is generated from Jupiter-family comets (JFCs), with additional minor contributions from main belt asteroids, Halley-type comets, Oort Cloud comets (OCCs), and interstellar dust (e.g., Nesvorný et al. 2010, 2011a, 2011b; Rowan-Robinson & May 2013; Pokorný et al. 2014). In situ dust detection has spanned from the inner (0.3–5 au) solar system (e.g., the *HELIOS* mission; Dietzel et al. 1973; Altobelli et al. 2006), into the outer (5–30 au) solar system (e.g., *Pioneer 10/11*, *Galileo*, *Ulysses*, and *Cassini*; Humes 1980; Grün et al. 1997; Altobelli et al. 2007), through the Edgeworth–Kuiper Belt (EKB; 30–100 au; e.g., *New Horizons*; Poppe et al. 2010; Piquette et al. 2019), and beyond (*Voyager 1/2*; Gurnett et al. 1997). Interpreted alongside various dynamical models (e.g., Kuchner & Stark 2010; Nesvorný et al. 2010, 2011a; Vitense et al. 2012; Poppe 2016), these data suggest that the interplanetary dust mass flux (summed from 0.5 to 500  $\mu\text{m}$ ) in our solar system is a heterogeneous mix from various parent bodies, transitioning from

<sup>8</sup> *New Horizons*/SDC Team.

JFC dominated inside 10 au, to OCC dominated between 10 and 30 au, and finally to EKB dominated outside of 30 au.

An outstanding goal in this field is to relate remote observations of exozodiacal debris disks to the structure and dynamics of our solar system’s debris disk and thereby place our mature system of age  $\sim 4.65$  Gyr in the context of planetary system formation and evolution. While the structure of the solar system’s inner debris disk (i.e., the zodiacal cloud) is relatively well studied, the outer debris disk in our solar system has only recently been fully explored in situ with a dedicated dust detector. With these new measurements in hand, we can now constrain system-wide models of the solar system’s debris disk much more quantitatively. Here, we present a comparison of recent *New Horizons* Student Dust Counter (SDC) interplanetary dust measurements out to 40 au with a dynamical dust model in order to constrain the interplanetary dust densities and bulk dust production rates. We then use the calibrated model to calculate the scattered light brightness, thermal emission brightness, spectral energy distribution (SED), and fractional luminosity of our debris disk in order to compare with other observed exozodiacal disks.

## 2. SDC Observations

Our best current knowledge of debris disk densities in the outer solar system comes from the Venetia Burney SDC on board the *New Horizons* mission (Horányi et al. 2008; Stern 2008). SDC is an impact-based dust detector that nominally faces the ram direction of the *New Horizons* spacecraft, is sensitive to grains with radii approximately between 0.5 and 5  $\mu\text{m}$  (depending on grain material density and the instantaneous dust grain and *New Horizons* velocities), and has taken measurements from  $\sim 2$  to 40 au heliocentric distance as of early 2019. Figure 1 shows (a) the *New Horizons*/SDC interplanetary trajectory with the minimum detectable dust grain mass denoted in color and (b) the SDC dust impact fluxes for grains larger than the minimum detectable mass threshold as a function of heliocentric distance, respectively. The minimum detectable mass increases as a function of heliocentric distance because the impact signal detected by SDC depends on impact velocity ( $\propto v^{2.88}$ ; James et al. 2010) and both the *New Horizons* spacecraft speed and average Keplerian dust grain speeds decrease as a function of heliocentric distance. Also shown in Figure 1(b) are model predictions for the interplanetary dust grain flux to *New Horizons*/SDC from the model of Poppe (2016) for the same minimum mass threshold (discussed further in Section 3). SDC has observed relatively flat impact fluxes of 0.5–5  $\mu\text{m}$  grains between 10 and 40 au, which via comparison to dynamical models that include dust contributions of asteroidal, cometary, and EKB sources (Nesvorný et al. 2010; Poppe 2016), are taken as strong evidence of the detection of ongoing dust grain production from an outer disk source such as EKB objects. Continued observations by *New Horizons*/SDC as it continues its cruise through the EKB should show decreasing interplanetary dust flux beginning around 45 au near the midpoint of the EKB. At 65 au, the model predicts interplanetary dust fluxes onto SDC to be an order of magnitude smaller than that within 45 au. The appearance of a gradual decline in interplanetary dust grain flux to SDC between 45 and 65 au should provide additional strong evidence of continuing dust grain production within the EKB, as opposed to a more distant, Oort Cloud source.

## 3. IDP Model Description

We now turn to a comparison of the latest SDC flux measurements with the interplanetary dust dynamics model of Poppe (2016) in order to constrain the full, large-scale structure of the solar system’s debris disk. The interplanetary dust particle (IDP) dynamics model uses a Bulirsch–Stoer integrator to track the dynamical evolution of individual dust grain test particles subject to several forces and processes, including solar and planetary gravitation, solar radiation pressure, Poynting–Robertson drag, solar wind drag, and the electromagnetic Lorentz force (assuming a constant +5 V charge on the grain and a simple Parker Spiral interplanetary magnetic field (IMF) model). Physical processes acting on the grains include charged particle sputtering, thermal sublimation, and grain–grain collisions. The dust dynamics model considers three main sources of interplanetary dust grains: JFCs, OCCs, and EKBs. Asteroidal, Halley-type cometary, and interstellar dust grains are also present throughout the solar system; however, previous work has shown their contributions to the overall dust disk mass to be minor (e.g., Grün et al. 1994; Nesvorný et al. 2010), and thus we do not include them here. We also note that active Centaurs, i.e., those objects with orbits between Jupiter and Neptune that have been observed to actively outgas material (e.g., Jewitt 2009; Epifani et al. 2011), may also contribute to interplanetary dust densities in the region; however, more detailed modeling of dust dynamics for grains released from these objects is needed to better quantify this potential source. Modeled grain radii range from 0.5  $\mu\text{m}$  (approximately at the blowout limit) to 500  $\mu\text{m}$ . As described in Poppe (2016), the modeled equilibrium density distributions for each IDP family have been previously constrained via a  $\chi^2$ -minimization comparison to *Pioneer 10* and *New Horizons*/SDC in situ measurements (Humes 1980; Poppe et al. 2010; Piquette et al. 2019) and correspond to total dust production rates for EKB, OCC, and JFC grains of  $3.5 \times 10^7 \text{ g s}^{-1}$ ,  $3 \times 10^5 \text{ g s}^{-1}$ , and  $5 \times 10^5 \text{ g s}^{-1}$ , respectively. The black dashed lines represent the best-fit models to the  $1\sigma$  error bars of the SDC data and mainly affect the rate of EKB dust production, which varies from  $1.6 \times 10^7$  to  $5.7 \times 10^7 \text{ g s}^{-1}$ . The best-fit fluxes to SDC are shown in Figure 1(b), both in terms of the total flux (black lines) and the separate contributions from EKB (green), OCC (blue), and JFC (orange) sources, respectively. Beyond approximately 5 au, SDC fluxes are dominated by grains derived from the EKB, providing strong evidence of ongoing dust production beyond Neptune.

### 3.1. Solar System Dust Disk Structures

Figures 2(a)–(c) show the face-on, 45°, and edge-on total geometric optical depth of the interplanetary dust distribution summed over dust type and over sizes from 0.5 to 500  $\mu\text{m}$ , respectively. Figures 2(d)–(f) show the relative contributions of EKB, OCC, and JFC dust grains to the optical depth as an *rgb* color blend, with the individual separate components as smaller insets to the right. The EKB optical depths display significant structure due in large part to planetary sculpting as expected from previous work (e.g., Liou & Zook 1999). The EKB optical depth is concentrated in a ring with  $\approx 10$  au thickness just exterior to Neptune’s orbit and extends beyond  $\sim 50$  au due to the presence of grains born from outer/detached EKB objects and from scattering of grains born from classical and/or resonant EKB objects by Neptune. The extension of EKB

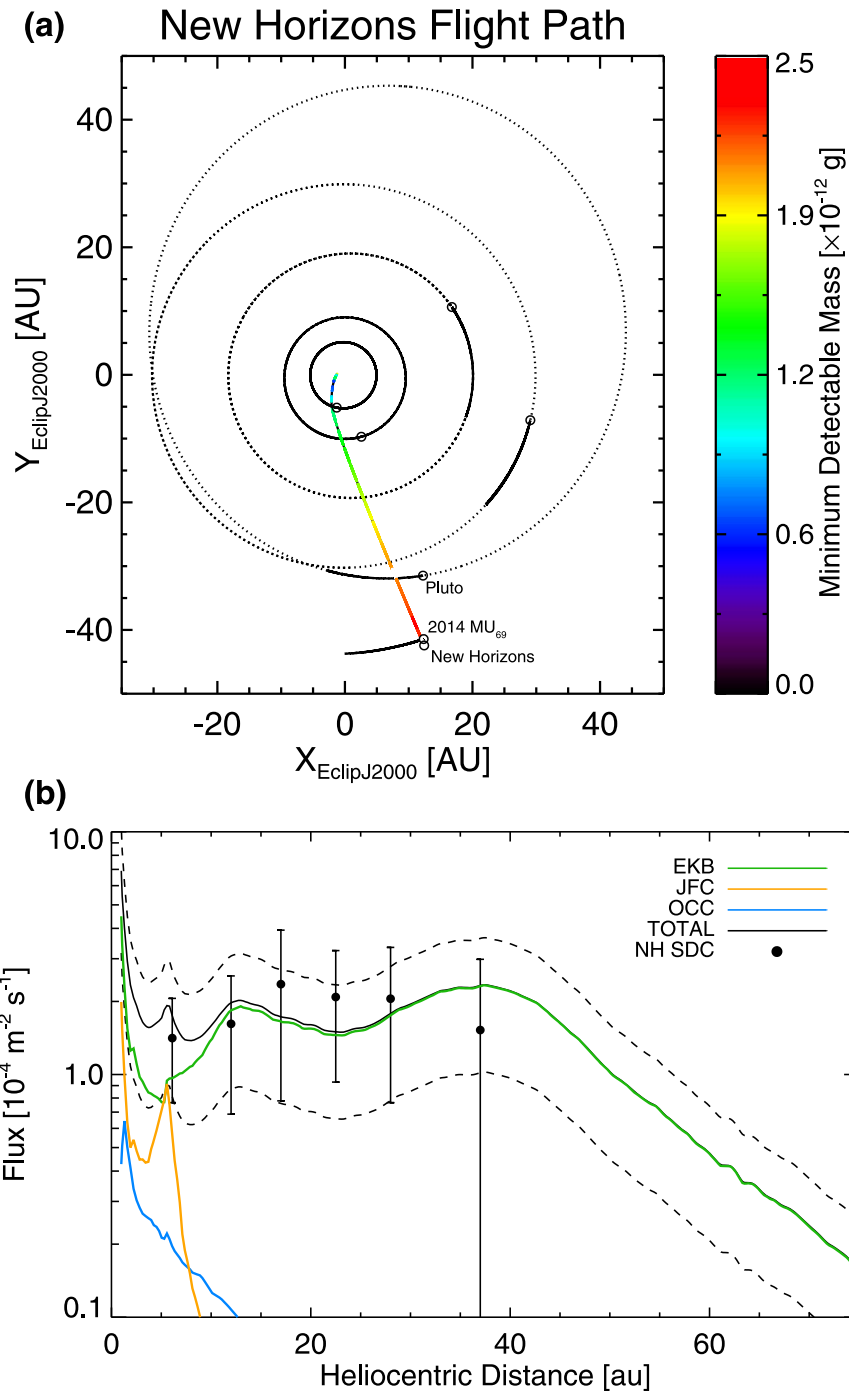


**Figure 1.** (a) The trajectory of *New Horizons* in the J2000 ecliptic plane. The orbits of the outer planets as well as Pluto and 2014 MU<sub>69</sub> are also denoted. Colors correspond to the minimum detectable dust grain mass (Piquette et al. 2019). (b) The measured SDC flux of grains between 0.5 and 5  $\mu\text{m}$  (solid points) compared to the best-fit model of Poppe (2016). The flattening of the measured dust flux at 10–40 au, after the initial very steep drop-off from 5 to 10 au as one traverses beyond the Jupiter-family cometary dust source, is telling of a second, outer belt source.

optical depth inward of Neptune is due to Poynting–Robertson and solar wind drag acting on the grains. EKB optical depths also possess a vertical (i.e., out-of-ecliptic) scale height of  $\approx 5$  au. EKB optical depths peak at  $3 \times 10^{-7}$ ,  $4.5 \times 10^{-7}$ , and  $2 \times 10^{-6}$  for each viewing angle (face-on,  $45^\circ$ , edge-on), respectively. OCC grains form a diffuse halo with no discernible structure, as gravitational perturbations are less significant considering the relatively high velocities of OCC grains. Peak OCC optical depths occur in the inner solar system at values of approximately  $8 \times 10^{-8}$ . JFC grains are mainly

confined within the orbit of Neptune with a distinct ring structure due to mean-motion resonance trapping with Jupiter near 5 au with peak optical depths of  $1.0 \times 10^{-7}$ ,  $1.4 \times 10^{-7}$ , and  $3 \times 10^{-7}$ , respectively. In sum, the optical depths at all three viewing angles display significant structure from both EKB and JFC grains due in large part to the presence of the outer planets (Liou & Zook 1999). In the ecliptic view, the total optical depth peaks at  $\approx 3 \times 10^{-7}$ , a factor of  $\approx 2$  higher than the model results of Kuchner & Stark (2010, their Figure 3, upper left), who obtained similar morphology with a peak

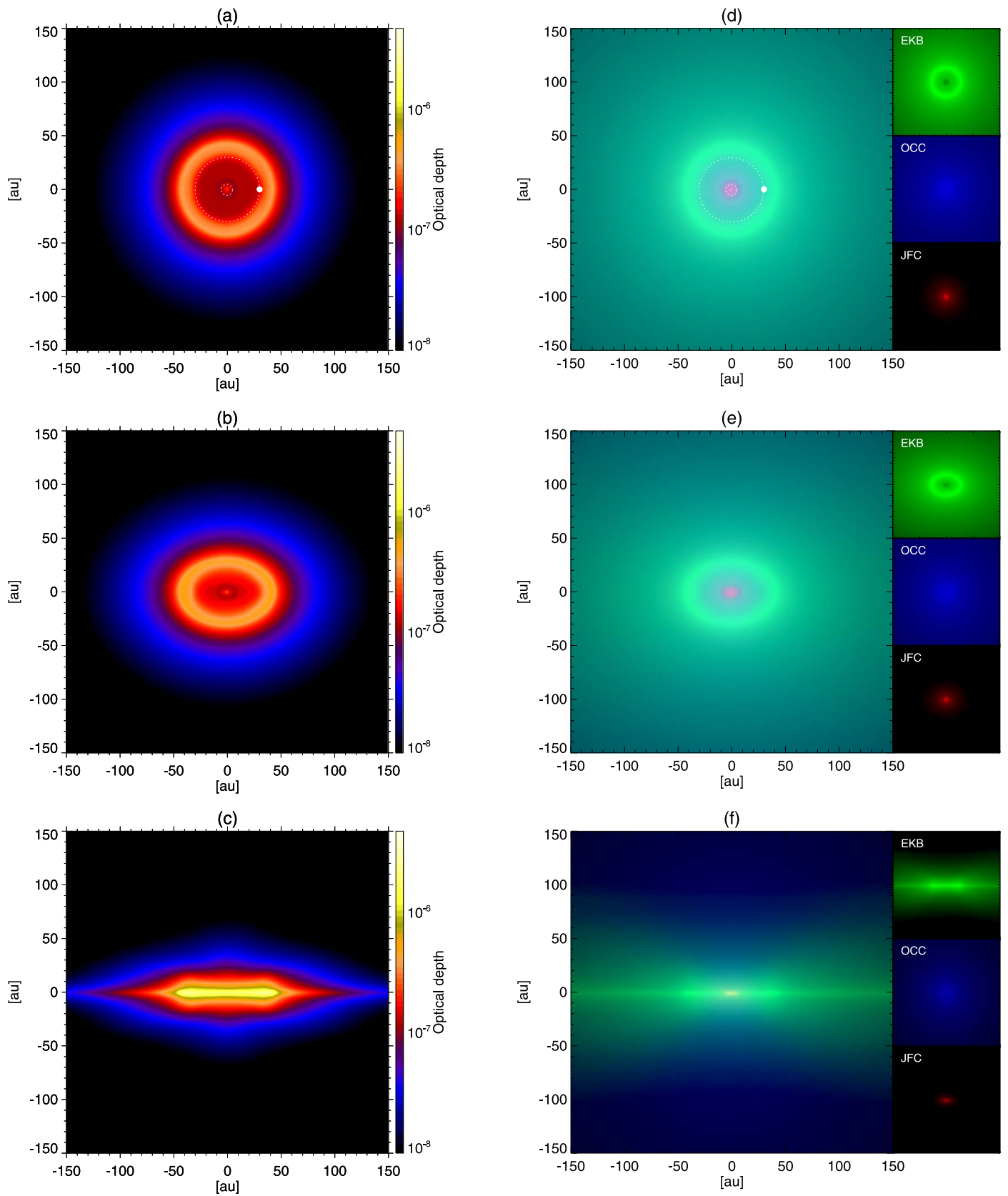


**Figure 2.** ((a)–(c)) The total geometric optical depth seen face-on, at  $45^\circ$ , and edge-on, respectively, using a logarithmic stretch. ((d)–(f)) The relative optical depths of EKB, OCC, and JFC grains shown as an *rgb* color blend, with individual components isolated in the smaller insets.

optical depth of  $\approx 1.3 \times 10^{-7}$ . In the meridional view, the total optical depth peaks at  $\approx 2.5 \times 10^{-6}$ , an order of magnitude higher than the ecliptic view.

#### 4. Modeled IDP Brightness

Using the modeled IDP densities, we have calculated both the scattered light brightness over wavelengths from 0.1 to 5  $\mu\text{m}$  and emitted thermal brightness over wavelengths from 20 to 500  $\mu\text{m}$  following the formalism of Augereau & Beust (2006) and Chen et al. (2008). Based on remote-sensing observations of cometary ejecta (e.g., Lisse et al. 2006, 2007b), we assume a dust composition of 25% olivine ( $\text{MgFeSiO}_4$ ), 25% enstatite ( $\text{MgSiO}_3$ ), and 50% amorphous carbon, using laboratory measurements of the optical constants for these three materials (Dorschner et al. 1995; Jäger et al. 1998, 2003). We note that while water ice may be a significant compositional component of interplanetary dust grains (e.g., Greenberg & Li 1999), processes such as photodesorption will rapidly erode any directly exposed water ice on grain surfaces (Grigorieva et al. 2007), removing its contribution to the grain’s optical properties; thus, we do not include a water ice component for this modeling exercise.

Figures 3(a)–(c) show the scattered light surface brightness for three wavelengths, 0.5, 1, and 3  $\mu\text{m}$ , as seen by an observer located above the ecliptic plane (i.e., phase angle of  $90^\circ$ ). The instantaneous position and orbit of Neptune are marked as the dot and dotted line, respectively. Scattered light brightness across this range of wavelengths peaks near  $10^{-1}$  MJy  $\text{sr}^{-1}$  in the inner solar system with dominant contributions there from JFC grains over OCC or EKB grains. Scattering from grains within the EKB ( $\sim 30$ – $50$  au) contributes to the scattered light brightness as a relatively diffuse, ring-like structure with maximum surface brightness on the order of  $10^{-4}$  MJy  $\text{sr}^{-1}$ . Figures 3(d)–(i) show the face-on view of the thermal emission surface brightness at six wavelengths: 5, 10, 50, 100, 200, and 500  $\mu\text{m}$ . The thermal emission surface brightness shows variation in structure as a function of observing wavelength. At the shorter end of the thermal emission wavelengths considered here, 5 and 10  $\mu\text{m}$ , the surface brightness peaks in the inner solar system at 50 MJy  $\text{sr}^{-1}$  mainly due to warmer JFC dust in the inner solar system. At wavelengths of 50  $\mu\text{m}$  and greater, emission from colder EKB grains becomes apparent in the region outside the orbit of Neptune, with peak surface brightnesses of  $10^{-1}$  MJy  $\text{sr}^{-1}$  at 50–100  $\mu\text{m}$ . The inner edge of EKB grain emission at 30 au is also clearly apparent, highlighting the effective role that Neptune plays in sculpting the outer dust disk (e.g., Liou & Zook 1999). At the longest wavelengths of 500  $\mu\text{m}$ , thermal brightnesses in both the inner solar system and the EKB drop to  $\sim 10^{-2}$  MJy  $\text{sr}^{-1}$ . While not shown in detail here, our model can also be used to estimate the line-of-sight surface brightness as seen by an observer at 1 au (e.g., similar to *IRAS*, *COBE*, and others). Assuming a line of sight in the ecliptic at  $90^\circ$  solar elongation, the model reasonably reproduces observed surface brightnesses at *COBE*/*DIRBE* wavelengths of 12, 24, 60, and 100  $\mu\text{m}$  (e.g., Kelsall et al. 1998; Fixsen & Dwek 2002). At these wavelengths, JFC dust dominates the modeled signal, with emission from EKB grains contributing no more than 10% of the overall signal. Future work will more quantitatively compare our model with the observations of *COBE*/*DIRBE* (e.g., Kelsall et al. 1998; Fixsen & Dwek 2002) and *Planck* (e.g., Maris et al. 2006; Planck Collaboration et al. 2014), for example.

Finally, Figure 4 shows the SED of the modeled solar system debris disk as observed from a distance of 1 pc, including the

solar spectrum (solid line; Labs & Neckel 1970; Neckel & Labs 1984), the debris disk scattered light contribution (dashed–dotted line), and the debris disk thermal emission contribution (dashed line). At a distance of 1 pc, the scattered light peaks at  $\approx 0.1$  mJy at 0.5  $\mu\text{m}$  and the thermal emission peaks at 50 mJy between 50 and 100  $\mu\text{m}$ . The peak thermal emission of 50 mJy derived here is consistent with previous model predictions by Kuchner & Stark (2010, their  $\tau_{\text{max}} = 10^{-7}$  case) and Vitense et al. (2012). Due to the inclusion of olivine and enstatite as constituent dust grain materials, silicate Si–O solid state vibrational features near 10 and 18  $\mu\text{m}$  are also apparent, albeit muted by the presence of spectrally flat amorphous carbon. The debris disk has a fractional flux of  $F_{\text{dust}}/F_{\odot} \sim 10^{-2}$  at its peak near 70  $\mu\text{m}$ , and summed over both scattered light and thermal emission, the fractional luminosity of our solar system’s debris disk is  $L_{\text{dust}}/L_{\odot} \sim 5 \times 10^{-7}$ .

#### 5. Discussion

Summing over masses between 0.5 and 500  $\mu\text{m}$ , our model finds total disk masses for the EKB, OCC, and JFC dust of  $3.5 \times 10^{18}$  kg ( $5.8 \times 10^{-7} M_{\oplus}$ ),  $1.3 \times 10^{18}$  kg ( $2.3 \times 10^{-7} M_{\oplus}$ ), and  $8.0 \times 10^{16}$  kg ( $1.3 \times 10^{-8} M_{\oplus}$ ), respectively. In total, the solar system’s debris disk consists of  $4.9 \times 10^{18}$  kg or  $8.2 \times 10^{-7} M_{\oplus}$ . If we restrict to those grains within 5 au, the total modeled disk mass is  $3.2 \times 10^{16}$  kg, dominated by JFC grains ( $>99\%$ ), and in good agreement with Nesvorný et al. (2010), who calculated an inner disk mass of approximately  $(1\text{--}2) \times 10^{16}$  kg. Summing over EKB, OCC, and JFC grains, the total debris disk mass is equivalent to an  $\sim 84$  km radius,  $2 \text{ g cm}^{-3}$  KBO that has been completely converted into submillimeter-sized dust; there are thought to be thousands of KBOs within this size range in the EKB today (Singer et al. 2019 and references therein). Interestingly, our model here estimates that  $\sim 70\%$  of the total interplanetary dust mass is contained with EKB grains and another  $\sim 27\%$  of the total mass is contained in OCC grains, nearly all of which lies outside 30 au. Thus, an observer taking a census of our debris disk from the outside would notice the overwhelming dust mass in the outer solar system, with the inner disk’s flux only apparent due to its close proximity to the central star. This is consistent with the low rate ( $\sim$ few percent) of warm asteroidal belts around FGK stars in the *WISE* survey (Patel et al. 2014) versus the higher,  $\sim 20\%$  detection frequency of exo-Kuiper Belts found in *Herschel* surveys of cold debris disks (Eiroa et al. 2013; Montesinos et al. 2016). Nevertheless, the solar system’s debris disk appears relatively dust-poor in comparison to debris disks around other  $\sim$ Gyr old FGK stars that possess disks with masses on the order of  $10^{-4}$ – $10^{-1} M_{\oplus}$  (e.g., Wyatt 2008, Figure 3) or 70  $\mu\text{m}$  fractional disk luminosities of  $10^0$ – $10^2$  (compared to  $10^{-2}$  for the solar system as shown in Figure 4; Wyatt 2008, Figure 10). On the other hand, we emphasize that this apparent relatively dust-poor nature of the solar system’s debris disk may be in part due to sensitivity limitations in debris disk surveys, for which a  $f_d \sim 5 \times 10^{-7}$  disk remains challenging to observe at distances  $> \sim 20$  pc (e.g., Montesinos et al. 2016), and to the mature, relatively dynamically cold, and “cleared-out” state of the modern solar system versus the dynamical instabilities driving massive dust production of the galaxy’s brightest exodisks.

We can connect our solar system’s debris disk to observed exo-debris disks in another way. All of the imaged exodisks, and the majority of the spectrally detected disks, are exo-Kuiper Belts formed from the edges of the respective systems’

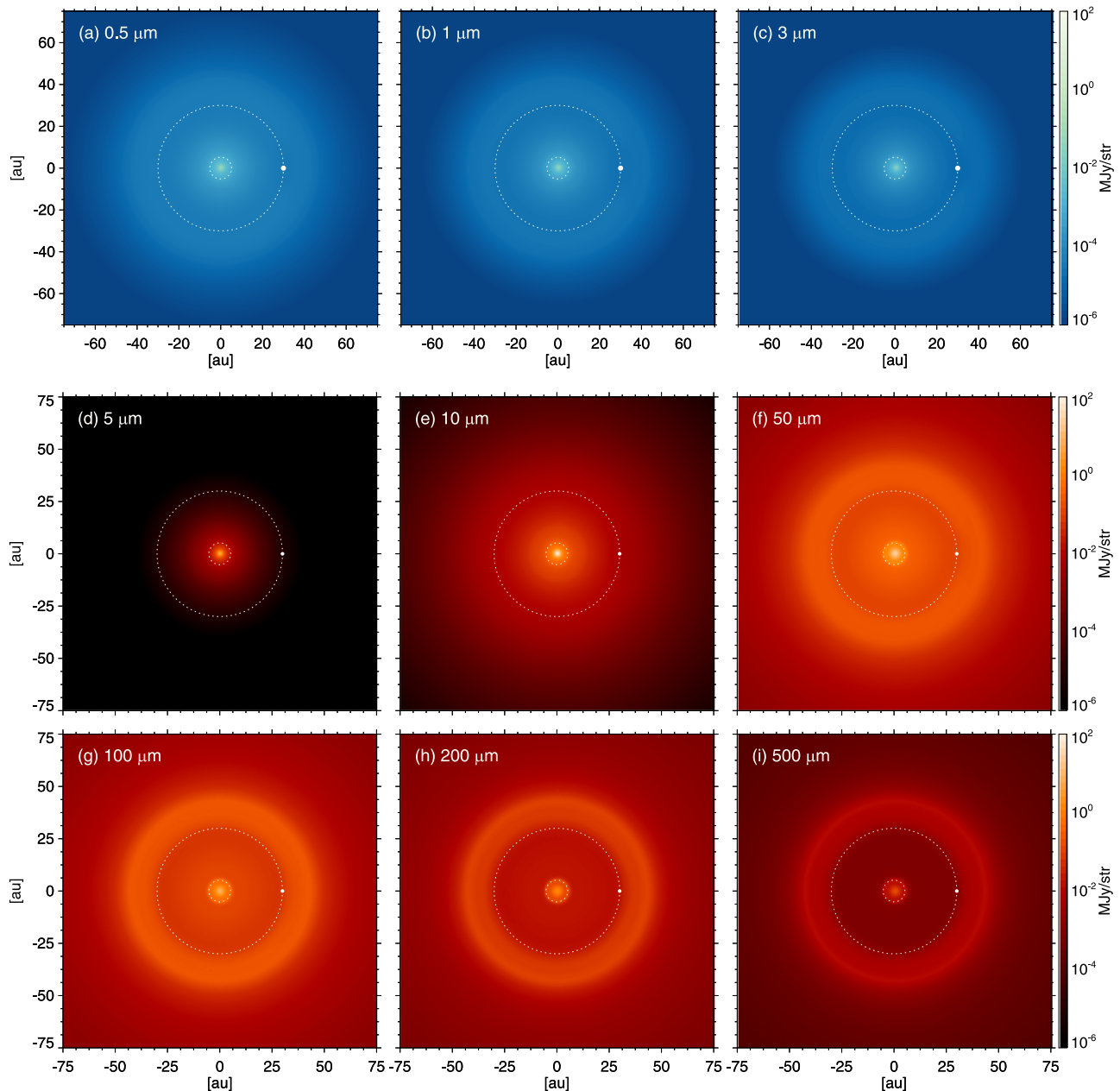


**Figure 3.** ((a)–(c)) Simulated scattered light brightness at 0.5, 1, and 3  $\mu\text{m}$ . ((d)–(i)) Simulated thermal emission surface brightness at 5, 10, 50, 100, 200, and 500  $\mu\text{m}$ . The two circular dashed lines mark the orbits of Jupiter and Neptune, respectively, while the white dot marks the position of Neptune in the Neptune-rotated frame used here.

protoplanetary disks. These disks can “brighten up,” making them easily seen if there are processes that create large amounts of new dust surface area. These processes include KBO aggregation (in young disks), disk stirring and enhanced collisional grinding (during planetary migration epochs in more mature disks), and KBO–KBO massive collisions/collisional family formation (in all exo-KB disks, but most important in the most mature). The disks become easily observed in scattered optical starlight if the processes produce fine  $\mu\text{m}$ -sized dust and more easily detected in thermal emission versus the primary star in the FIR/submillimeter if the processes produce copious amounts of millimeter–centimeter-sized dust fragments. Here, we focus on collisional grinding and family formation processes. We have a direct analogy for this process in our solar system: the formation of our main belt collisional

asteroid families, and their ties to the band structures seen in the solar system’s zodiacal dust cloud (Nesvorný et al. 2006; Espy Kehoe et al. 2015). We have another direct analogy in a nearby system for the brightening of a disk via recent asteroid family formation in the HD 69830 system (Lisse et al. 2007a; Beichman et al. 2011) and for ongoing collisional dust formation in the distant ID8 asteroid family analogy (e.g., Meng et al. 2012, 2014).

So how to tie the above observations to Kuiper Belts, as opposed to asteroid belts? There is one reported collisional family in our Kuiper Belt, namely, the Haumea family (e.g., Brown et al. 2007; Schlichting & Sari 2009). The estimated total amount of mass in solid bodies in this family system is  $4.1 \times 10^{24}$  g, with 97% of it in Haumea and 3% of it in collisional fragments (Proudford & Ragozzine 2019), and if we

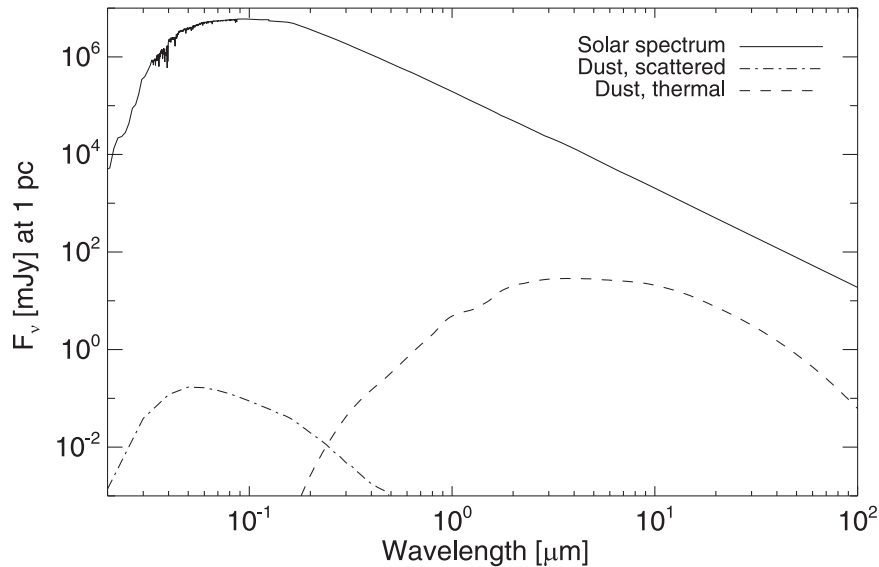


**Figure 4.** Modeled spectral emission distribution including scattered light, thermal emission, and the solar spectrum (Labs & Neckel 1970; Neckel & Labs 1984), respectively.

assume that another 3% of mass went into dust production at the time of collision, we have  $\sim 1.2 \times 10^{23}$  g of dust created by the family formation event. This amount of dust is  $\sim 35\times$  the present-day total EKB dust mass calculated here, and if we naively (neglecting, for example, the expected changes in dust disk morphology due to higher grain–grain collision frequencies; e.g., Kuchner & Stark 2010) scale our modeled EKB dust disk mass by a factor of  $35^{2/3}$  (since  $\pi a^2 \propto m^{2/3}$ ), the dust disk brightness in the infrared increases by a factor of  $\sim 6\times$ . If we were to apply the same exercise to a hypothetical collisional event with the current most massive KBO, Eris, with a mass of  $1.6 \times 10^{25}$  g (or four times the mass of Haumea), the EKB debris disk would brighten by a factor of  $\sim 15\times$  over the current one. In these two cases (Haumea and Eris), the  $12 \mu\text{m}$  fractional excesses become  $6.0 \times 10^{-4}$  and  $1.4 \times 10^{-3}$  (compared to  $1.2 \times 10^{-4}$ ), well below that detected in the HOSTS survey (Ertel et al. 2018). Additionally, the  $70 \mu\text{m}$  fractional excess rises from  $1.5 \times 10^{-2}$  to 0.095 and 0.2, respectively, placing the solar system debris disk at the extreme lower end of observed  $70 \mu\text{m}$  fractional excesses (Wyatt 2008, Figure 10) for debris disks around nearby Sun-like stars for ages  $\sim 1$  Gyr (since the Haumea formation event is believed to be primordial; Ragozzine & Brown 2007). This fact can be interpreted as evidence in support of the hypothesis that much of the Kuiper Belt’s primordial mass was removed during the Late Heavy Bombardment planetary instability (e.g., Morbidelli et al. 2004; Gomes et al. 2005). By corollary, we can suppose that  $>1$  Gyr old systems with bright Kuiper Belts are undergoing strong self-stirring and collisional cascade processes (e.g., Krivov & Booth 2018) and/or perhaps never formed an outer planet capable of migrating and scattering remanent planetesimals out of the primordial exo-Kuiper Belt.

## 6. Conclusion

We have used the latest *New Horizons* SDC measurements to further constrain the interplanetary dust grain distribution in both the inner and outer solar system and, using these constraints, have built a robust model of the scattered light and thermal emission brightness expected from our solar system’s debris

disk. *New Horizons* SDC measurements (Piquette et al. 2019) have proven invaluable in demonstrating the ongoing production of micron-sized dust grains from the EKB. As discussed previously in Poppe (2016) and demonstrated here in Figure 1(b), SDC flux measurements beyond  $\sim 10$  au are best fit by production from a source external to Neptune as opposed to cometary outgassing in the inner solar system by Jupiter-family comets and OCCs. A similar conclusion was drawn earlier by Landgraf et al. (2002) based on *Pioneer 10* and *11* meteoroid detector measurements out to 18 au. We conclude by stating the additional remote-sensing and in situ measurements of the solar system’s debris disk and, in particular, the outer solar system component of the debris disk, are necessary to advance our understanding. The *Cassini* Dust Analyzer (Srama et al. 2004) has over 13 years of observations of interplanetary dust particle fluxes at 10 au that, if properly isolated from Saturnian system dust (e.g., Kempf et al. 2008), can provide powerful dynamical and compositional constraints on the outer solar system dust environment. Furthermore, continued analysis of scattered light images taken from *New Horizons* on its voyage to Pluto may also reveal a signal from outer solar system dust (e.g., Zemcov et al. 2017). Finally, future spacecraft that visit the outer solar system should consider the addition of instruments capable of either remote-sensing observations in the visible to infrared or capable of in situ impact-based dust detection.

A.R.P. and M.Z. acknowledge the NASA New Frontiers Data Analysis Program, grant #80NSSC18K1557. C.M.L. acknowledges the support and input of the NASA Nexus for Exoplanet System Science (NExSS) research coordination network sponsored by NASA’s Science Mission Directorate. The authors also acknowledge the immense effort of the *New Horizons* team in successfully guiding the mission, including the Student Dust Counter, across the solar system.

## ORCID iDs

A. R. Poppe  <https://orcid.org/0000-0001-8137-8176>  
 C. M. Lisse  <https://orcid.org/0000-0002-9548-1526>  
 M. Zemcov  <https://orcid.org/0000-0001-8253-1451>

## References

- Altobelli, N., Dikarev, V., Kempf, S., et al. 2007, *JGRA*, **112**, A07105
- Altobelli, N., Grün, E., & Landgraf, M. 2006, *A&A*, **448**, 243
- Augereau, J.-C., & Beust, H. 2006, *A&A*, **455**, 987
- Aumann, H. H. 1985, *PASP*, **97**, 885
- Aumann, H. H., Gillett, F. C., Beichman, C. A., et al. 1984, *ApJL*, **278**, L23
- Beichman, C. A., Lisse, C. M., Tanner, A. M., et al. 2011, *ApJ*, **743**, 85
- Borkowski, K. J., & Dwek, E. 1995, *ApJ*, **454**, 254
- Brown, M. E., Barkume, K. M., Ragozzine, D., & Schaller, E. L. 2007, *Natur*, **446**, 294
- Burns, J. A., Lamy, P. L., & Soter, S. 1979, *Icar*, **40**, 1
- Chen, C. H., Fitzgerald, M. P., & Smith, P. S. 2008, *ApJ*, **689**, 539
- Chiang, E., Kite, E., Kalas, P., et al. 2009, *ApJ*, **693**, 734
- Dietzel, H., Eichhorn, G., Fechtig, H., et al. 1973, *JPhE*, **6**, 209
- Dikarev, V. V., & Schwarz, D. J. 2015, *A&A*, **584**, A9
- Dorschner, J., Begemann, B., Henning, T., et al. 1995, *A&A*, **300**, 503
- Eiroa, C., Marshall, J. P., Mora, A., et al. 2013, *A&A*, **555**, A11
- Epifani, E. M., Dall’Ora, M., Perna, D., Palumbo, P., & Colangeli, L. 2011, *MNRAS*, **415**, 3097
- Ertel, S., Defrere, D., Hinz, P., et al. 2018, *AJ*, **155**, 194
- Espy Kehoe, A. J., Kehoe, T. J. J., Colwell, J. E., & Dermott, S. F. 2015, *ApJ*, **811**, 66
- Fixsen, D. J., & Dwek, E. 2002, *ApJ*, **578**, 1009
- Gomes, R., Levison, H. F., Tsiganis, K., & Morbidelli, A. 2005, *Natur*, **435**, 466
- Greaves, J. S., Holland, W. S., Moriarty-Schieven, G., et al. 1998, *ApJL*, **506**, L133
- Greaves, J. S., Holland, W. S., Wyatt, M. C., et al. 2005, *ApJL*, **619**, L187
- Greenberg, J. M., & Li, A. 1999, *SSRv*, **90**, 149
- Grigorieva, A., Thébault, P., Artymowicz, P., & Brandeker, A. 2007, *A&A*, **475**, 755
- Grün, E., Gustafson, B., Mann, I., et al. 1994, *A&A*, **286**, 915
- Grün, E., Staubach, P., Baguhl, M., et al. 1997, *Icar*, **129**, 270
- Gurnett, D. A., Ansher, J. A., Kurth, W. S., & Granroth, L. J. 1997, *GeoRL*, **24**, 3125
- Gustafson, B. A. S. 1994, *AREPS*, **22**, 553
- Hahn, J. M., Zook, H. A., Cooper, B., & Sunkara, B. 2002, *Icar*, **158**, 360
- Hanner, M. S., Weinberg, J. L., DeShields, L. M., II, et al. 1974, *JGR*, **79**, 3671
- Hauser, M. G., Gillett, F. C., Low, F. J., et al. 1984, *ApJL*, **278**, L15
- Horányi, M., Hoxie, V., James, D., et al. 2008, *SSRv*, **140**, 387
- Hughes, A. M., Duchêne, G., & Matthews, B. C. 2018, *ARA&A*, **56**, 541
- Humes, D. H. 1980, *JGR*, **85**, 5841
- Jäger, C., Dorschner, J., Mutschke, H., et al. 2003, *A&A*, **408**, 193
- Jäger, C., Mutschke, H., & Henning, T. 1998, *A&A*, **332**, 291
- James, D., Horányi, M., & Hoxie, V. 2010, *RSci*, **81**, 034501
- Jewitt, D. 2009, *AJ*, **137**, 4296
- Kelsall, T., Weiland, J. L., Franz, B. A., et al. 1998, *ApJ*, **508**, 44
- Kempf, S., Beckmann, U., Moragas-Klostermeyer, G., et al. 2008, *Icar*, **193**, 420
- Kondo, T., Ishihara, D., Kaneda, H., et al. 2016, *AJ*, **151**, 71
- Kral, Q., Krivov, A. V., Defrère, D., et al. 2017, *AstRv*, **13**, 69
- Krivov, A. V., & Booth, M. 2018, *MNRAS*, **479**, 3300
- Kuchner, M. J., & Stark, C. C. 2010, *AJ*, **140**, 1007
- Labs, D., & Neckel, H. 1970, *SoPh*, **15**, 79
- Landgraf, M., Liou, J.-C., Zook, H. A., & Grün, E. 2002, *AJ*, **123**, 2857
- Liou, J.-C., & Zook, H. A. 1999, *AJ*, **118**, 580
- Lisse, C. M., Beichman, C. A., Bryden, G., & Wyatt, M. C. 2007a, *ApJ*, **658**, 584
- Lisse, C. M., Kraemer, K. E., Nuth, J. A., III, et al. 2007b, *Icar*, **187**, 69
- Lisse, C. M., VanCleve, J., Adams, A. C., et al. 2006, *Sci*, **313**, 635
- Maris, M., Burigana, C., & Fogliani, S. 2006, *A&A*, **452**, 685
- Meng, H. Y. A., Rieke, G. H., Su, K. Y. L., et al. 2012, *ApJL*, **751**, L17
- Meng, H. Y. A., Su, K. Y. L., Rieke, G. H., et al. 2014, *Sci*, **345**, 1032
- Montesinos, B., Eiroa, C., Krivov, A. V., et al. 2016, *A&A*, **593**, A51
- Morbidelli, A., Brown, M. E., & Levison, H. F. 2004, in *The First Decadal Review of the Edgeworth–Kuiper Belt*, ed. J. K. Davies & L. H. Barrera (Dordrecht: Springer), **1**
- Neckel, H., & Labs, D. 1984, *SoPh*, **90**, 205
- Nesvorný, D., Janches, D., Vokrouhlický, D., et al. 2011a, *ApJ*, **743**, 129
- Nesvorný, D., Jenniskens, P., Levison, H. F., et al. 2010, *ApJ*, **713**, 816
- Nesvorný, D., Vokrouhlický, D., Bottke, W. F., & Sykes, M. 2006, *Icar*, **181**, 107
- Nesvorný, D., Vokrouhlický, D., Pokorný, P., & Janches, D. 2011b, *ApJ*, **743**, 37
- Patel, R. I., Metchev, S. A., & Heinze, A. 2014, *ApJS*, **212**, 10
- Piquette, M., Poppe, A. R., Bernardoni, E., et al. 2019, *Icar*, **321**, 116
- Planck Collaboration, Ade, P. A. R., Aghanim, N., et al. 2014, *A&A*, **571**, A14
- Pokorný, P., Vokrouhlický, D., Nesvorný, D., et al. 2014, *ApJ*, **789**, 25
- Poppe, A., James, D., Jacobsmeyer, B., & Horányi, M. 2010, *GeoRL*, **37**, L11101
- Poppe, A. R. 2016, *Icar*, **264**, 369
- Proudford, B. C. N., & Ragozzine, D. 2019, *AJ*, **157**, 230
- Ragozzine, D., & Brown, M. E. 2007, *AJ*, **134**, 2160
- Reach, W. T., Abergel, A., Boulanger, F., et al. 1996, *A&A*, **315**, L381
- Reach, W. T., Morris, P., Boulanger, F., & Okumura, K. 2003, *Icar*, **164**, 384
- Rowan-Robinson, M., & May, B. 2013, *MNRAS*, **429**, 2894
- Schlichting, H. E., & Sari, R. 2009, *ApJ*, **700**, 1242
- Singer, K. N., McKinnon, W. B., Gladman, B., et al. 2019, *Sci*, **363**, 955
- Srama, R., Ahrens, T. J., Altobelli, N., et al. 2004, *SSRv*, **114**, 465
- Stark, C. C., & Kuchner, M. J. 2008, *ApJ*, **686**, 637
- Stern, S. A. 2008, *SSRv*, **140**, 3
- Vitense, C., Krivov, A. V., Kobayashi, H., & Löhne, T. 2012, *A&A*, **540**, A30
- Wyatt, M. C. 2003, *ApJ*, **598**, 1321
- Wyatt, M. C. 2008, *ARA&A*, **46**, 339
- Wyatt, M. C., Dermott, D. F., Telesco, C. M., et al. 1999, *ApJ*, **527**, 918
- Zemcov, M., Immel, P., Nguyen, C., et al. 2017, *NatCo*, **8**, 15003



# Erratum: “Constraining the Solar System’s Debris Disk with In Situ *New Horizons* Measurements from the Edgeworth-Kuiper Belt” (2019, *ApJL*, 881, L12)

A. R. Poppe<sup>1,8</sup> , C. M. Lisse<sup>2</sup> , M. Piquette<sup>3,8</sup>, M. Zemcov<sup>4</sup> , M. Horányi<sup>5,8</sup>, D. James<sup>5,8</sup>, J. R. Szalay<sup>6,8</sup> ,  
E. Bernardoni<sup>5,8</sup>, and S. A. Stern<sup>7,8</sup>

<sup>1</sup> Space Sciences Laboratory, University of California at Berkeley, 7 Gauss Way, Berkeley, CA, 94720, USA; [poppe@ssl.berkeley.edu](mailto:poppe@ssl.berkeley.edu)

<sup>2</sup> Johns Hopkins University Applied Physics Laboratory, Laurel, MD, USA

<sup>3</sup> Laboratory for Atmospheric and Space Physics, University of Colorado at Boulder, Boulder, CO 80309, USA

<sup>4</sup> Center for Detectors, School of Physics and Astronomy, Rochester Institute of Technology, 1 Lomb Memorial Drive, Rochester, NY 14623, USA

<sup>5</sup> Dept. of Physics and Laboratory for Atmospheric and Space Physics, University of Colorado at Boulder, Boulder, CO 80309, USA

<sup>6</sup> Department of Astrophysical Sciences, Princeton University, Princeton, NJ, USA

<sup>7</sup> Southwest Research Institute, Boulder, CO, USA

Received 2019 August 18; published 2019 September 3

## 1. Introduction

In the original Letter, the abscissa values in Figure 4 were inadvertently off by one order of magnitude. The corrected Figure 1 is shown below. This error did not affect the discussion or conclusions in the original Letter.

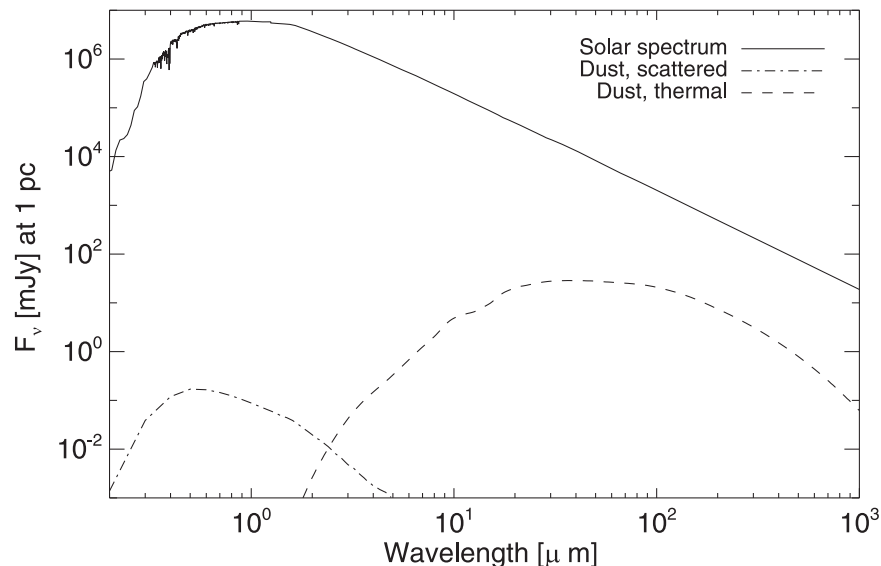


**Figure 1.** The modeled spectral emission distribution including both scattered light, thermal emission, and the solar spectrum (Labs & Neckel 1970; Neckel & Labs 1984), respectively.

## ORCID iDs

A. R. Poppe  <https://orcid.org/0000-0001-8137-8176>

C. M. Lisse  <https://orcid.org/0000-0002-9548-1526>

M. Zemcov  <https://orcid.org/0000-0001-8253-1451>

J. R. Szalay  <https://orcid.org/0000-0003-2685-9801>

## References

Labs, D., & Neckel, H. 1970, *SoPh*, 15, 79

Neckel, H., & Labs, D. 1984, *SoPh*, 90, 205

<sup>8</sup> *New Horizons*/SDC Team.